



King's Research Portal

DOI:

[10.1016/j.jtcvs.2016.09.040](https://doi.org/10.1016/j.jtcvs.2016.09.040)

Document Version

Peer reviewed version

[Link to publication record in King's Research Portal](#)

Citation for published version (APA):

Youssefi, P., Gomez, A., He, T., Anderson, L., Bunce, N., Sharma, R., Figueroa, C. A., & Jahangiri, M. (2016). Patient-Specific Computational Fluid Dynamics – Assessment of Aortic Hemodynamics in a Spectrum of Aortic Valve Pathologies. *Journal of Thoracic and Cardiovascular Surgery*. <https://doi.org/10.1016/j.jtcvs.2016.09.040>

Citing this paper

Please note that where the full-text provided on King's Research Portal is the Author Accepted Manuscript or Post-Print version this may differ from the final Published version. If citing, it is advised that you check and use the publisher's definitive version for pagination, volume/issue, and date of publication details. And where the final published version is provided on the Research Portal, if citing you are again advised to check the publisher's website for any subsequent corrections.

General rights

Copyright and moral rights for the publications made accessible in the Research Portal are retained by the authors and/or other copyright owners and it is a condition of accessing publications that users recognize and abide by the legal requirements associated with these rights.

- Users may download and print one copy of any publication from the Research Portal for the purpose of private study or research.
- You may not further distribute the material or use it for any profit-making activity or commercial gain
- You may freely distribute the URL identifying the publication in the Research Portal

Take down policy

If you believe that this document breaches copyright please contact librarypure@kcl.ac.uk providing details, and we will remove access to the work immediately and investigate your claim.

Accepted Manuscript

Patient-Specific Computational Fluid Dynamics – Assessment of Aortic Hemodynamics in a Spectrum of Aortic Valve Pathologies

Pouya Youssefi, BSc(Hons) MBBS MRCS(Eng), Alberto Gomez, PhD, Taigang He, PhD, Lisa Anderson, MBBS MRCP, Nick Bunce, MBBS MRCP, Rajan Sharma, MBBS MRCP, C. Alberto Figueroa, PhD, Marjan Jahangiri, FRCS(CTh)

PII: S0022-5223(16)31158-8

DOI: [10.1016/j.jtcvs.2016.09.040](https://doi.org/10.1016/j.jtcvs.2016.09.040)

Reference: YMTC 10908

To appear in: *The Journal of Thoracic and Cardiovascular Surgery*

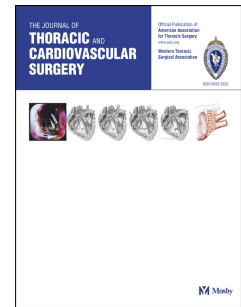
Received Date: 12 February 2016

Revised Date: 24 August 2016

Accepted Date: 14 September 2016

Please cite this article as: Youssefi P, Gomez A, He T, Anderson L, Bunce N, Sharma R, Figueroa CA, Jahangiri M, Patient-Specific Computational Fluid Dynamics – Assessment of Aortic Hemodynamics in a Spectrum of Aortic Valve Pathologies, *The Journal of Thoracic and Cardiovascular Surgery* (2016), doi: [10.1016/j.jtcvs.2016.09.040](https://doi.org/10.1016/j.jtcvs.2016.09.040).

This is a PDF file of an unedited manuscript that has been accepted for publication. As a service to our customers we are providing this early version of the manuscript. The manuscript will undergo copyediting, typesetting, and review of the resulting proof before it is published in its final form. Please note that during the production process errors may be discovered which could affect the content, and all legal disclaimers that apply to the journal pertain.



Patient-Specific Computational Fluid Dynamics – Assessment of Aortic Hemodynamics in a Spectrum of Aortic Valve Pathologies

Pouya Youssefi, BSc(Hons) MBBS MRCS(Eng)^{1,2}; Alberto Gomez, PhD²; Taigang He, PhD¹; Lisa Anderson, MBBS MRCP¹; Nick Bunce, MBBS MRCP¹; Rajan Sharma, MBBS MRCP¹; C. Alberto Figueroa, PhD^{2,3}; Marjan Jahangiri, FRCS(CTh)¹

¹ Department of Cardiothoracic Surgery & Cardiology, St. George's Hospital, St. George's University of London, Blackshaw Road, London, SW17 0QT, United Kingdom.

² Department of Biomedical Engineering, King's College London, London SE1 7EH, United Kingdom.

³ Departments of Surgery and Biomedical Engineering, University of Michigan, Ann Arbor, MI 48109 USA.

Corresponding Author:

Marjan Jahangiri

Email: marjan.jahangiri@stgeorges.nhs.uk

Tel: (44) 20 8725 3565

Fax: (44) 20 8725 2049

Address: Marjan Jahangiri, FRCS
Department of Cardiothoracic Surgery
St. George's Hospital
Blackshaw Road
London, SW17 0QT
United Kingdom

Manuscript Word Count: 3500 words

Funding Sources

This work was supported by the European Research Council under the European Union's Seventh Framework Programme FP/2007-2013 / European Research Council (Grant Agreement no. 307532 to A.F.), British Heart Foundation New Horizons program (NH/11/5/29058 to A.F.), the Royal College of Surgeons of England Research Fellowship (to P.Y.), the United Kingdom Department of Health via the National Institute for Health Research (NIHR) comprehensive Biomedical Research Centre award to Guy's & St Thomas' NHS Foundation Trust in partnership with King's College London and King's College Hospital NHS Foundation Trust.

Disclosures

None.

ABSTRACT

Objectives: The complexity of aortic disease is not fully exposed by aortic dimensions alone, and morbidity or mortality can occur before intervention thresholds are met. Patient-specific computational fluid dynamics (CFD) was used to assess effect of different aortic valve morphologies on velocity profiles, flow patterns, helicity, wall shear stress (WSS) and oscillatory shear index (OSI) in the thoracic aorta.

Methods: 45 subjects were divided into 5 groups: Volunteers, AR-TAV, AS-TAV, AS-BAV(RL), AS-BAV(RN), where AR=aortic regurgitation, AS=aortic stenosis, TAV=tricuspid aortic valve, BAV=bicuspid aortic valve, RL=right-left cusp fusion, RN=right-non cusp fusion. Subjects underwent magnetic resonance angiography, with phase-contrast MRI at the sino-tubular junction to define patient-specific inflow velocity profiles. Hemodynamic recordings were used alongside MRI angiographic data to run patient-specific CFD.

Results: BAV groups had larger mid-ascending aorta diameters ($p<0.05$). Ascending aorta flow was more eccentric in BAV ($\text{Flow}_{\text{asymmetry}}=78.9\pm6.5\%$ for AS-BAV(RN), compared to $4.7\pm2.1\%$ for Volunteers, $p<0.05$). Helicity was higher in AS-BAV(RL) ($p<0.05$). Mean WSS was elevated in AS groups, highest in AS-BAV(RN) ($37.1\pm4.0 \text{ dyn/cm}^2$, compared to 9.8 ± 5.4 for Volunteers, $p<0.05$). The greater curvature of the ascending aorta experienced highest WSS and lowest OSI in AS patients, most significant in AS-BAV(RN) ($p<0.05$).

Conclusions: BAV displays eccentric flow with high helicity. Presence of AS, particularly in BAV-RN led to higher WSS and lower OSI in the greater curvature of the ascending aorta.

Patient-specific CFD provides non-invasive functional assessment of the thoracic aorta, and may enable development of a personalized approach to diagnosis and management of aortic disease beyond traditional guidelines.

Abstract Word Count: 247 words

68 **Abbreviations**

69	CFD	=	Computational fluid dynamics
70	WSS	=	Wall shear stress
71	OSI	=	Oscillatory shear index
72	BAV	=	Bicuspid aortic valve
73	TAV	=	Tricuspid aortic valve
74	AS	=	Aortic stenosis
75	AR	=	Aortic regurgitation
76	AV	=	Aortic valve
77	CMR	=	Cardiovascular magnetic resonance
78	HFI	=	Helical flow index

79

Central Message

Patient-specific CFD reveals high WSS and lower OSI in the greater curvature of BAV aortas, with highly eccentric and helical flow.

Perspective Statement

In patients with AV disease and aortic aneurysm, morbidity or mortality can occur before size criteria for intervention are met. Patient-specific CFD provides non-invasive functional and hemodynamic assessment of the thoracic aorta. With validation it may enable development of an individualized approach to diagnosis and management of aortic disease beyond traditional guidelines.

INTRODUCTION

For many years, treatment guidelines and intervention criteria have concentrated on traditional echocardiographic measurements for the aortic valve (AV).^{1, 2} Furthermore, size remains the principal decision-making index for treatment of the thoracic aorta.^{3, 4} However, there is growing evidence that hemodynamics play an important role in aneurysm formation, with effects on endothelial homeostasis, smooth muscle response, and fibroblast function.^{5, 6}

Flow characteristics are highly variable in the thoracic aorta, where the inflow velocity profile is largely dependent on the morphology of the AV. Bicuspid aortic valve (BAV) is the most common congenital cardiac abnormality with an estimated prevalence of 1-2%, as well as a morbidity and mortality accounting for more than that of all other congenital cardiac diseases combined.⁷ BAV is often associated with aneurysms of the ascending aorta or aortic root. This dilatation can lead to eventual dissection or rupture.⁸

Disease processes such as aneurysm formation and atherosclerosis are greatly affected by hemodynamic factors in the vascular system.⁹⁻¹² Spatial velocity gradients together with blood viscosity result in wall shear stresses on the endothelium. Wall shear stress (WSS) refers to the force per unit area exerted by a moving fluid in the direction of the local tangent of the luminal surface.¹³ Lower WSS has been observed in those carotid arteries with higher levels of plaque formation.¹⁴ In contrast, high wall shear stress has been associated with aneurysm formation in the cerebral arteries.¹⁵ Oscillatory shear index (OSI) is a metric that quantifies the changes in direction and magnitude of WSS and has been associated with vasculopathy.¹⁶ It ranges between 0 (in uni-directional steady flow) and 0.5 (perfectly oscillating back-and-forth velocities over the cardiac cycle). Flow in the thoracic aorta has a

significant helical component due to a combination of factors such as ventricular twist and torsion,¹⁷ mechanics of the AV and aortic root, and the curved morphology of the aortic arch.¹⁸ This helical flow has been related to both plaque deposition¹⁹ and aneurysm formation.²⁰ These hemodynamic and biomechanical parameters can be measured non-invasively using computational fluid dynamics (CFD).

In this study, we aimed to use patient-specific CFD to assess the effect of different AV morphologies on velocity profiles, flow patterns and helicity, wall shear stress and oscillatory shear index in the thoracic aorta.

METHODS

Study Population

45 subjects were studied. They were divided into the following 5 groups: Volunteers – healthy volunteers with tricuspid aortic valves (n=5); AR-TAV – aortic regurgitation tricuspid aortic valves (n=10); AS-TAV – aortic stenosis tricuspid aortic valves (n=10); AS-BAV(RL) – aortic stenosis bicuspid aortic valves with fusion of right and left coronary cusps (n=10); AS-BAV(RN) – aortic stenosis bicuspid aortic valves with fusion of right and non-coronary cusps (n=10). Diagnosis of AS or AR was based on trans-thoracic echocardiographic data. AS was defined as aortic $V_{max} > 4$ m/s, mean pressure gradient > 40 mmHg, AV area < 1.0 cm², or AV area index < 0.6 cm²/m². AR was defined as jet width $> 65\%$ of left ventricular outflow tract, vena contracta ≥ 0.6 cm, regurgitant volume > 60 ml/beat, or effective regurgitant orifice ≥ 0.3 cm².¹ Patients with coarctation were excluded. The study was approved by the local ethical committee (St. George's University of London, equivalent to IRB), and informed consent was gained from all healthy volunteers and patients.

Imaging

Patients underwent standard of care Cardiac Magnetic Resonance (CMR) imaging and Magnetic Resonance Angiography (MRA) to image the entire thoracic aorta, including the head and neck vessels.

Time-resolved, velocity encoded 2D anatomic and through-plane PC-MRI (flow MRI) was performed on a plane orthogonal to the ascending aorta at the sino-tubular junction. Heart rates amongst subjects ranged between 50-95 bpm during which 30 images were reconstructed. Cine sequences were performed for assessment of valve morphology. Velocity sensitivity was set between 150 to 500 cm/s depending on the degree of AS. Average scan times were 20 minutes. Supine bilateral upper blood pressure (BP) assessment was performed using a Dinamap system (GE Healthcare, Waukesha, WI). See Appendix A for details of the MRI imaging techniques.

Computational Fluid Dynamics

Three-dimensional geometric models of the thoracic aorta were reconstructed from the MRA data using custom software (<http://www.crimson.software/>).²¹ A tetrahedral mesh was created by discretising the geometric model of the aorta to produce anisotropic meshes consisting of approximately 2.5 to 5.5 million elements. Blood flow simulations were carried out using a stabilized finite element formulation to solve equations enforcing conservation of mass (continuity) and balance of linear momentum (Navier-Stokes) for the flow of an incompressible Newtonian fluid with density $\rho = 1.06 \text{ g/cm}^3$ and dynamic viscosity $\mu = 0.04$ Poise.²² The validated in-house code CRIMSON was used for this process (<http://www.crimson.software/>).²¹

The flow-MRI data was used to define the patient-specific inflow velocity profile. An in-house software written in *Matlab* (The Mathworks Inc., Massachusetts, USA) was used to

extract velocity profiles from the flow-MR images and map them to the inlet face of the aortic model.

The outflow boundary conditions were carried out in a patient-specific manner using blood pressure recordings and cardiac output measurements from the flow-MRI data. A coupled-multi-domain formulation was utilized whereby 3-element Windkessel models (comprising of a proximal resistance (R_p), compliance (C), and a distal resistance (R_d)) were coupled to each outflow branch (e.g., innominate artery, left common carotid artery, left subclavian artery, and descending aorta) (Appendix B).²³

Quantification of Hemodynamic Indices

Velocity maps (2D) and velocity profiles (3D) were extracted from the PC-MRI data above the AV (see figure 1). Flow asymmetry ($\text{Flow}_{\text{asymmetry}}$) was acquired by measuring the distance between the centroid of the top 15% of peak systolic velocities ($V_{\text{max}}^{15\%}$) and the geometric centroid of the inlet plane, as a percentage of the equivalent radius of the inlet plane. A $\text{Flow}_{\text{asymmetry}}$ of 0% means flow is central to the axis of the vessel, and a $\text{Flow}_{\text{asymmetry}}$ of 100% means flow is completely eccentric and at the periphery of the lumen (see figure 1).

Aortic 3D velocity streamlines were calculated from temporally resolved 3D velocity data for the entire thoracic aorta, and colour coded by blood velocity magnitude. Helicity is a metric that represents the extent to which corkscrew-like motion occurs, and is governed by velocity

and vorticity. Helical Flow Index (HFI) was calculated to quantitatively measure the degree of helicity according to Hardman et al.¹⁶

WSS and OSI were obtained for the entire thoracic aorta, with further in-depth sub-analysis in the ascending aorta. In order to look for asymmetry and differences in WSS and OSI on different sides of the aorta, the ascending aorta was divided into 8 anatomical sectors (anterior (A), right-anterior (RA), right (R), right-posterior (RP), posterior (P), left-posterior (LP), left (L), and left-anterior (LA) sectors; see figure 2).

The results were visualised using the open-source software ParaView (Kitware, Inc., Clifton Park, NY). Further details on how HFI, WSS and OSI were calculated are included in Appendix C.

Statistical Analysis

Data is presented as mean \pm standard deviation. For each group, data was tested for Gaussian distribution using the Shapiro-Wilk test. One-way analysis of variance (ANOVA) was used to test for difference in results between groups. If this revealed $p < 0.05$, multiple comparisons were carried out between all groups using independent-sample t tests. A p value < 0.01 was considered significant following Bonferroni correction to adjust for multiple comparisons. All statistical analysis was carried out using SPSS (version 21, IBM).

RESULTS

Patient Demographics

The degree of AS or AR met the severity criteria described above in all patients except for the Volunteers group, who were chosen for their normal functioning AVs. The demographics and aortic dimensions for the 5 groups are displayed in Table 1. Both BAV groups had larger mid-ascending aortic diameters compared to Volunteers ($p < 0.01$).

Velocity Patterns

Figure 3 depicts 2D velocity maps and 3D velocity profiles above the AV for a representative subject from each of the 5 groups. When AS is present, the 3D velocity profiles are very peaked and narrow, compared to the broader velocity profiles of Volunteers and AR-TAV. BAV patients show high velocity in the periphery of the lumen, whereas TAV patients display more central velocity jets. BAV patients had $\text{Flow}_{\text{asymmetry}}$ almost twice the magnitude of the TAV patients, indicating blood flow was much more eccentric and asymmetrical (table 1).

Helicity

The Volunteers group show laminar flow patterns with relatively uniform parallel 3D velocity streamlines indicating undisrupted flow (figure 4). AS-TAV and AR-TAV show a slightly higher degree of helical flow compared to the Volunteers group. BAV patients

display the most degree of cork-screw like helical flow and high velocity jets travelling in a spiral manner around the ascending aorta and arch. Helicity of blood flow in the ascending aorta was assessed by the Helical Flow Index (HFI), which at peak systole was significantly higher in the AS-BAV(RL) group (see table 1).

Wall Shear Stress

Figure 5 shows cycle-averaged, or mean WSS (MWSS) maps throughout the thoracic aorta for each of the 5 groups. The 3 groups with AS show high levels of MWSS in the ascending aorta, predominantly affecting the greater curvature. Volunteers and AR-TAV show lower levels of MWSS. Table 1 shows the values of MWSS averaged over the ascending aorta ($MWSS^{Asc\ Aorta}$). $MWSS^{Asc\ Aorta}$ was similar in Volunteers and AR-TAV. AS-BAV(RN) showed the highest $MWSS^{Asc\ Aorta}$ at $37.1 \pm 4.0 \text{ dyn/cm}^2$.

For each subject, the ascending aorta was divided into 8 sectors circumferentially. WSS averaged for each sector at each time point was plotted against time over the cardiac cycle (figure 6). For Volunteers and AR-TAV, WSS plots are low in magnitude and the curves remain close together throughout the cardiac cycle, indicating relatively symmetrical and uniform WSS distribution around the ascending aorta. In contrast, the 3 AS groups (AS-BAV(RL), AS-BAV(RN) and AS-TAV), show higher WSS plots in the first one-third of the cardiac cycle (corresponding to systole). The sectors displaying high WSS are the right-anterior (RA) and right (R) sectors for the BAV patients, and the anterior (A), right-anterior (RA), and right (R) sectors for the TAV aortic stenosis patients. This indicates significantly asymmetrical WSS distribution.

The 3-dimensional radar plots shown in figure 7 reveal an asymmetrical distribution of MWSS around the circumference of the ascending aorta in the 3 AS groups. When comparing between groups, MWSS in the anterior (A), right-anterior (RA) and right (R) sectors for AS-BAV(RN) is statistically higher when compared to Volunteers and AR-TAV ($p < 0.01$). MWSS in the right-anterior (RA) sector for AS-BAV(RL) is higher when compared to Volunteers (but only achieving $p < 0.05$).

Oscillatory Shear Index

Ascending aorta oscillatory shear index ($OSI^{Asc\ Aorta}$) is lower in AS-BAV(RN) ($OSI^{Asc\ Aorta} = 0.13 \pm 0.02$, compared to 0.18 ± 0.03 for AS-BAV(RL), 0.19 ± 0.02 for AS-TAV, 0.21 ± 0.04 for AR-TAV, and 0.18 ± 0.04 for Volunteers). Only the Volunteers showed symmetrical OSI values in the ascending aorta. Both bicuspid groups showed relatively lower OSI levels in the right-anterior (RA) sectors. For AS-BAV(RN), this was statistically significant for the anterior (A), right-anterior (RA) and right (R) sectors when compared to Volunteers ($p < 0.01$). The tricuspid patients (AS-TAV and AR-TAV) have higher OSI levels on the left side of the aorta, with a significantly higher OSI in the left-anterior (LA) sector for AS-TAV when compared to AS-BAV(RN) ($p < 0.01$) (see figure 7).

DISCUSSION

The results from this study show that the presence of BAV was associated with eccentric blood flow patterns and high helicity. AS, whether bicuspid or tricuspid, led to higher WSS levels in the ascending aorta, with the WSS distribution being asymmetrical and highest in AS-BAV(RN). OSI was also asymmetrically distributed, with the lowest levels found in patients with AS-BAV(RN). These findings corresponded with larger mid-ascending aorta diameters in BAV patients.

Implications for Management Guidelines

The results of this study question whether a patient-specific functional assessment of the thoracic aorta should be undertaken instead of size measurements alone. Guidelines of intervention on the aorta consist of maximal aortic diameter as the principal management criteria, with treatment recommended at smaller diameters in the presence of risk factors such as connective tissue disorders or family history of dissection.³ These criteria have remained largely unchanged for many years. However despite these guidelines, there is still an incidence of rupture or dissection when the aorta is below these size criteria. Elefteriades et al. have shown the yearly risk of rupture, dissection or death to be 4.4%, 4.7%, 7.3% and 12.1% for aortic sizes 4, 5, 6 and 7 cm respectively.²⁴ This shows that there remains a small but significant incremental risk of aortic events for those patients with aortic size below current intervention criteria.

These findings also provide new insights into the adequacy of traditional long-standing indices of valve assessment. Maximum aortic velocity, pressure gradients, valve area, regurgitant volumes and vena contracta are some of the established echocardiographic indices used to assess AV function.² Whilst some of these hemodynamic indices relate to symptoms and signs of aortic valve pathology, and assess its effect on the left ventricle, they do not help in the assessment of aortic valve-related aortopathy. There is as of yet no robust functional assessment of the effect of the AV on the aorta, both in terms of flow changes and mechanical stresses. Evidence shows a strong association between BAV and aneurysm of the ascending aorta, with a risk of subsequent dissection or rupture.⁸ Yet the decision of when to intervene surgically on this group of patients can be difficult. The degree of aortic dilatation can be highly variable, and management guidelines are supported by limited evidence. It is not uncommon to be presented with a BAV patient who has an intermediate severity of valve dysfunction and a moderate degree of aortic dilatation. This patient may not fulfil current criteria for surgical intervention on the AV or the aorta, however assessment of some of the functional indices outlined in this study may help decision making.

Valve Morphology & Hemodynamics

Wall shear stress was higher in the presence of AS, whether BAV or TAV. MWSS was highest in the right-non fusion BAV patients. The WSS distribution was highly asymmetrical, with the right-anterior (RA) and right (R) sectors experiencing the highest levels of WSS. These sectors correlate with the convexity (greater curvature) of the ascending aorta. It was interesting to note that both BAV groups had significantly larger mid-ascending aorta

diameters compared to Volunteers. These trends are in keeping with earlier CFD studies,^{25, 26} although our results are based on larger patient numbers, less hemodynamic assumptions, and more patient-specific parameters. 4D flow MRI studies by Mahadevia et al. also found WSS to be higher in sectors corresponding to the greater curvature of the ascending aorta in patients with BAV.²⁷ Meierhofer et al. also used 4D flow MRI and measured WSS to be up to 7.5 dyn/cm² (0.75 N/m²) in the ascending aorta of healthy tricuspid valve patients,²⁸ corresponding to 9.8 ± 5.4 dyn/cm² measured in our study. WSS measurements for BAV patients in their study were higher than TAV patients, but were not as high as the levels seen in our study. This may be due to lack of aortic stenosis or insufficiency in their BAV patients. Our results also correlate well with the findings of Della Corte et al. who found that medial degeneration was more severe in the greater curvature of BAV aortas.²⁹ Type I and III collagen were reduced in this area. Smooth muscle cell apoptosis was seen to be increased in the greater curvature of BAV aortas even before significant dilatation had occurred.³⁰ Oscillatory shear index throughout the ascending aorta was lower in the right-non BAV group. When comparing the 8 sectors, lower OSI was seen in the A, RA and R sectors. Higher OSI has been associated with increased atherosclerotic plaque formation, and an increase in vessel wall thickness.³¹ It may be postulated that this lower OSI seen in AS-BAV(RN) may be protective from atherosclerotic plaques, or perhaps to even cause thinning of the wall. The 3 sectors which demonstrated lower OSI were those corresponding to the greater curvature of the ascending aorta, typically the site of wall thinning.²⁹ Further work in this area may lend additional insights into the mechanisms of aortopathy.

As the morphology of the AV changed relative to healthy volunteers, blood flow helicity increased. There was a step-wise increase in helicity from Volunteer → TAV (AS or AR) → AS-BAV(RN) → AS-BAV(RL). This may be related to the asymmetrical flow seen in BAV patients. Helicity has been shown to play an important role in plaque deposition¹⁹ and aneurysm formation.²⁰ High helicity has been linked with high WSS, in part due to the non-axial velocity component as well as its link with disrupted flow.^{32, 33} This trend was also seen in our results.

This work has been focused on hemodynamic indices in the aorta and their correlation to known vasculopathies. Pressure, on the other hand, is the most important contributor to tensile stress, the key determinant in aneurysm rupture when wall stress exceeds wall strength. WSS acts in the direction of the vessel wall and is governed by velocity. It is a smaller quantity compared to tensile stress³⁴ and the tensile strength³⁵ of the aortic wall (Pascals for WSS compared to hundreds of kiloPascals for tensile stress), however interacts with the vessel wall via different mechanisms. Tensile stress could be estimated by Finite Element Modelling of the aorta using appropriate constitutive models to describe the characteristics of the wall.

Future Application of CFD

Current assessment of patients with aortopathy is largely limited to surveillance of aortic size by CT or MRA. There remains a lack of information regarding each patient's aortic wall biomechanics and flow patterns. Indices such as WSS and OSI have been shown to be associated with aneurysm formation/rupture¹⁵ and vasculopathy.¹⁶ This study found WSS to

be highest and OSI to be lowest in the greater curvature of the ascending aorta of bicuspid patients, the site of typical dilatation and thinning.²⁹ Further investigations should include longitudinal studies to assess the correlation between the proposed hemodynamic indices and aortopathy events, as well as the effect of these indices on proteomic changes, gene expression, and inflammatory changes in the aortic wall. Knowledge of these parameters may then help highlight those patients at higher risk of aortic complications, and help guide timing of surgical intervention.

4D flow MRI can also be used to assess some of these hemodynamic parameters, however due to lower spatial and temporal resolution, underestimation of WSS is a recognised problem.³⁶ Furthermore, 4D flow MRI has a longer acquisition time which may be inconvenient for the patient. The MRA and PC-MRI image acquisition required to carry out CFD is of significantly shorter duration.

CFD is a non-invasive approach to quantify biomechanics and hemodynamics in assessment of aortic pathology. Future development and incorporation of CFD algorithms and tools into imaging modality systems may give clinicians access to each patient's individual aortic flow dynamics and biomechanics.

Limitations

The results from this study have not been adjusted for patient characteristics such as age. Future studies should contain different AV morphology groups such as aortic regurgitation BAV, and even mixed AV disease groups (mixed AS and AR). Furthermore, a comparison of

BAV morphologies with different degrees of stenosis or regurgitation should be made to assess hemodynamic parameters in bicuspid patients with less than severe AS or AR.

Computations were performed under the assumption of rigid walls. Increasing compliance and elasticity causes a small reduction in WSS, so our results may have over-estimated WSS in all 5 groups. As the aorta dilates, its compliance and elasticity reduce, and it becomes stiffer and more rigid. This makes it more susceptible to higher shear stresses, and increases the risk of rupture or dissection.³⁷ The 2 bicuspid groups in this study had significantly larger aortas, and it may be suggested that the aortic wall may have been stiffer than the smaller diameter tricuspid groups. Therefore, WSS would have been proportionally more over-estimated in the TAV groups. Thus the actual differences in WSS between BAV and TAV groups could have been even higher than that seen in this study. In future studies, fluid-structure interaction analysis that takes into account the elasticity of the aortic wall will be performed.

CONCLUSIONS

The outcomes in aortic hemodynamics from this study may relate to a potential explanation for the increased incidence of aortopathy in BAV patients, and indeed to some degree of post-stenotic dilatation seen in some TAV aortic stenosis patients. Our results show that there are increased velocity jets found at the periphery of the aorta in BAV patients. Velocity streamlines show that these narrow jets impact on the greater curvature of the ascending

aorta, and subsequently spiral around the ascending aorta and arch. They cause increased wall shear stress and reduced oscillatory shear index at the greater curvature, corresponding to larger mid-ascending aorta diameters. These findings provide a possible mechanistic link between aortic valve morphology and aortopathy. CFD is a non-invasive functional assessment of the thoracic aorta, and may enable development of an improved personalized approach to the diagnosis and management of aortic disease beyond traditional guidelines.

402 **Acknowledgements**

403 The authors acknowledge support from Desmond Dillon-Murphy and Dr. Christopher
404 Arthurs for their expertise and technical assistance.

405

406

References

1. Nishimura RA, Otto CM, Bonow RO, Carabello BA, Erwin JP, 3rd, Guyton RA, et al. 2014 AHA/ACC guideline for the management of patients with valvular heart disease: a report of the American College of Cardiology/American Heart Association Task Force on Practice Guidelines. *J Am Coll Cardiol*. 2014;63:e57-185.
2. Vahanian A, Alfieri O, Andreotti F, Antunes MJ, Baron-Esquivias G, Baumgartner H, et al. Guidelines on the management of valvular heart disease (version 2012): the Joint Task Force on the Management of Valvular Heart Disease of the European Society of Cardiology (ESC) and the European Association for Cardio-Thoracic Surgery (EACTS). *Eur J Cardiothorac Surg*. 2012;42:S1-44.
3. Erbel R, Aboyans V, Boileau C, Bossone E, Bartolomeo RD, Eggebrecht H, et al. 2014 ESC Guidelines on the diagnosis and treatment of aortic diseases: Document covering acute and chronic aortic diseases of the thoracic and abdominal aorta of the adult. The Task Force for the Diagnosis and Treatment of Aortic Diseases of the European Society of Cardiology (ESC). *Eur Heart J*. 2014;35:2873-926.
4. Svensson LG, Adams DH, Bonow RO, Kouchoukos NT, Miller DC, O'Gara PT, et al. Aortic valve and ascending aorta guidelines for management and quality measures. *Ann Thorac Surg*. 2013;95:S1-66.
5. Gnasso A, Carallo C, Irace C, Spagnuolo V, De Novara G, Mattioli PL, et al. Association between intima-media thickness and wall shear stress in common carotid arteries in healthy male subjects. *Circulation*. 1996;94:3257-62.

- 428 6. Malek AM, Alper SL and Izumo S. Hemodynamic shear stress and its role in
429 atherosclerosis. *JAMA*. 1999;282:2035-42.
- 430 7. Ward C. Clinical significance of the bicuspid aortic valve. *Heart*. 2000;83:81-5.
- 431 8. Della Corte A, Bancone C, Quarto C, Dialetto G, Covino FE, Scardone M, et al.
432 Predictors of ascending aortic dilatation with bicuspid aortic valve: a wide spectrum of
433 disease expression. *Eur J Cardiothorac Surg*. 2007;31:397-404.
- 434 9. Friedman MH, Hutchins GM, Barger CB, Deters OJ and Mark FF. Correlation
435 between intimal thickness and fluid shear in human arteries. *Atherosclerosis*. 1981;39:425-
436 36.
- 437 10. Zarins CK, Giddens DP, Bharadvaj BK, Sottiurai VS, Mabon RF and Glagov S.
438 Carotid bifurcation atherosclerosis. Quantitative correlation of plaque localization with flow
439 velocity profiles and wall shear stress. *Circ Res*. 1983;53:502-14.
- 440 11. Yeung JJ, Kim HJ, Abbruzzese TA, Vignon-Clementel IE, Draney-Blomme MT,
441 Yeung KK, et al. Aortoiliac hemodynamic and morphologic adaptation to chronic spinal cord
442 injury. *J Vasc Surg*. 2006;44:1254-1265.
- 443 12. Humphrey JD and Taylor CA. Intracranial and abdominal aortic aneurysms:
444 similarities, differences, and need for a new class of computational models. *Annu Rev Biomed*
445 *Eng*. 2008;10:221-46.
- 446 13. Efstathiopoulos EP, Patatoukas G, Pantos I, Benekos O, Katritsis D and Kelekis NL.
447 Wall shear stress calculation in ascending aorta using phase contrast magnetic resonance
448 imaging. Investigating effective ways to calculate it in clinical practice. *Phys Med*.
449 2008;24:175-81.

14. Gnasso A, Irace C, Carallo C, De Franceschi MS, Motti C, Mattioli PL, et al. In vivo association between low wall shear stress and plaque in subjects with asymmetrical carotid atherosclerosis. *Stroke*. 1997;28:993-8.
15. Cebal JR, Vazquez M, Sforza DM, Houzeaux G, Tateshima S, Scrivano E, et al. Analysis of hemodynamics and wall mechanics at sites of cerebral aneurysm rupture. *J Neurointerv Surg*. 2015;7:530-6.
16. Hardman D, Semple SI, Richards JM and Hoskins PR. Comparison of patient-specific inlet boundary conditions in the numerical modelling of blood flow in abdominal aortic aneurysm disease. *Int J Numer Method Biomed Eng*. 2013;29:165-78.
17. Baciewicz FA, D. G. Penney, W. A. Marinelli, and and Marinelli. R. Torsional ventricular motion and rotary blood flow. What is the clinical significance. *Cardiac Chronicle*. 1991;5:1-8.
18. Chandran KB. Flow dynamics in the human aorta. *J Biomech Eng*. 1993;115:611-6.
19. Kilner PJ, Yang GZ, Mohiaddin RH, Firmin DN and Longmore DB. Helical and retrograde secondary flow patterns in the aortic arch studied by three-directional magnetic resonance velocity mapping. *Circulation*. 1993;88:2235-47.
20. Hope MD, Hope TA, Crook SE, Ordovas KG, Urbania TH, Alley MT, et al. 4D flow CMR in assessment of valve-related ascending aortic disease. *JACC Cardiovasc Imaging*. 2011;4:781-7.
21. Figueroa C, Khlebnikov R, Lau KD, Arthurs CJ, Dillon-Murphy D, Alastruey-Armon J, et al. www.crimson.software.

22. Figueroa CA, Vignon-Clementel IE, Jansen KC, Hughes TJ and Taylor CA. A coupled momentum method for modeling blood flow in three-dimensional deformable arteries. *Comput Methods Appl Mech Eng.* 2006;195:5685-5706.
23. Vignon-Clementel IE, Figueroa CA, Jansen KE and Taylor CA. Outflow boundary conditions for 3D simulations of non-periodic blood flow and pressure fields in deformable arteries. *Comput Methods Biomech Biomed Engin.* 2010;13:625-40.
24. Elefteriades JA, Ziganshin BA, Rizzo JA, Fang H, Tranquilli M, Paruchuri V, et al. Indications and imaging for aortic surgery: size and other matters. *J Thorac Cardiovasc Surg.* 2015;149:S10-3.
25. Rinaudo A and Pasta S. Regional variation of wall shear stress in ascending thoracic aortic aneurysms. *Proc Inst Mech Eng H.* 2014;228:627-638.
26. Viscardi F, Vergara C, Antiga L, Merelli S, Veneziani A, Puppini G, et al. Comparative finite element model analysis of ascending aortic flow in bicuspid and tricuspid aortic valve. *Artif Organs.* 2010;34:1114-20.
27. Mahadevia R, Barker AJ, Schnell S, Entezari P, Kansal P, Fedak PW, et al. Bicuspid aortic cusp fusion morphology alters aortic three-dimensional outflow patterns, wall shear stress, and expression of aortopathy. *Circulation.* 2014;129:673-82.
28. Meierhofer C, Schneider EP, Lyko C, Hutter A, Martinoff S, Markl M, et al. Wall shear stress and flow patterns in the ascending aorta in patients with bicuspid aortic valves differ significantly from tricuspid aortic valves: a prospective study. *Eur Heart J Cardiovasc Imaging.* 2013;14:797-804.
29. Della Corte A, De Santo LS, Montagnani S, Quarto C, Romano G, Amarelli C, et al. Spatial patterns of matrix protein expression in dilated ascending aorta with aortic

regurgitation: congenital bicuspid valve versus Marfan's syndrome. *J Heart Valve Dis.*

2006;15:20-7.

30. Della Corte A, Quarto C, Bancone C, Castaldo C, Di Meglio F, Nurzynska D, et al.

Spatiotemporal patterns of smooth muscle cell changes in ascending aortic dilatation with

bicuspid and tricuspid aortic valve stenosis: focus on cell-matrix signaling. *J Thorac*

Cardiovasc Surg. 2008;135:8-18.

31. Campbell IC, Ries J, Dhawan SS, Quyyumi AA, Taylor WR and Oshinski JN. Effect

of inlet velocity profiles on patient-specific computational fluid dynamics simulations of the

carotid bifurcation. *J Biomech Eng.* 2012;134:051001.

32. Morbiducci U, Ponzini R, Grigioni M and Redaelli A. Helical flow as fluid dynamic

signature for atherogenesis risk in aortocoronary bypass. A numeric study. *J Biomech.*

2007;40:519-34.

33. Frazin LJ, Vonesh MJ, Chandran KB, Shipkowitz T, Yaacoub AS and McPherson

DD. Confirmation and initial documentation of thoracic and abdominal aortic helical flow.

An ultrasound study. *ASAIO J.* 1996;42:951-6.

34. Fillinger MF, Marra SP, Raghavan ML and Kennedy FE. Prediction of rupture risk in

abdominal aortic aneurysm during observation: wall stress versus diameter. *J Vasc Surg.*

2003;37:724-32.

35. Ferrara A, Morganti S, Totaro P, Mazzola A and Auricchio F. Human dilated

ascending aorta: Mechanical characterization via uniaxial tensile tests. *J Mech Behav Biomed*

Mater. 2016;53:257-71.

36. Barker AJ, Markl M, Burk J, Lorenz R, Bock J, Bauer S, et al. Bicuspid aortic valve is associated with altered wall shear stress in the ascending aorta. *Circ Cardiovasc Imaging*. 2012;5:457-66.
37. Xiong G, Figueroa CA, Xiao N and Taylor CA. Simulation of blood flow in deformable vessels using subject-specific geometry and spatially varying wall properties. *Int J Numer Method Biomed Eng*. 2011;27:1000-1016.

Figure Legends

Central Picture. Mean wall shear stress (MWSS) map of right-non fusion BAV patient.

Figure 1. (a) 2D velocity map above the AV showing areas of different velocity represented by colour; (b) 3D velocity profile showing a warped geometric representation of the velocity pattern; (c) and (d) velocity map and velocity profile showing $V_{\max}^{15\%}$ (the top 15% of velocities at peak systole) in red dots. The yellow sphere is the centroid of the whole plane, whereas the blue sphere is the centroid of $V_{\max}^{15\%}$. $\text{Flow}_{\text{asymmetry}}$ is calculated by dividing distance x by distance y as a percentage.

Figure 2. The ascending aorta is divided into 8 anatomical segments for sub-analysis of hemodynamic parameters. A = anterior; RA = right-anterior; R = right; RP = right-posterior; P = posterior; LP = left-posterior; L = left; LA = left-anterior. RCA = right coronary artery; LCA = left coronary artery.

Figure 3. (a) schematic diagram of AV morphology in the 5 study groups; (b) 2D velocity maps above the AV at peak systole; (c) 3D velocity profiles above the AV at peak systole; (d) 3D schematic of the location of the top 15% of velocity at peak systole ($V_{\max}^{15\%}$), as shown in red; (e) 2D map of the location of $V_{\max}^{15\%}$ (white circle = centroid of inflow, yellow circle = centroid of $V_{\max}^{15\%}$). RCA = right coronary artery, LCA = left coronary

artery.

Figure 4. 3D velocity streamlines showing trajectory of velocity during peak systole for example patients from the 5 study groups. Higher velocity jets are represented by red colour.

Figure 5. Mean wall shear stress (MWSS) maps for example patients from the 5 study groups. The MWSS maps look at the thoracic aorta from 2 different views. Red colour represents areas of high WSS.

Figure 6. Wall shear stress (WSS) plots throughout the cardiac cycle for example patients from each of the 5 groups. Each line represents one of the 8 anatomical sectors of the ascending aorta. Abbreviations as in figure 2

Figure 7. (a) Plots of mean wall shear stress (MWSS) for each of the 8 sectors of the ascending aorta. Error bars represent standard deviations of MWSS. **(b)** Radial graphs of oscillatory shear index (OSI) for each of the 8 sectors of the ascending aorta. * indicates statistically significant differences for AS-BAV(RN) cohorts in comparison with AR-TAV and AR-TAV ($p < 0.01$). ϕ represents statistically significant differences for AS-TAV cohorts in comparison with AS-BAV(RN) ($p < 0.01$). ψ represents differences for AS-BAV(RL) cohorts in comparison with AR-TAV ($p < 0.05$). Abbreviations as in figure 2.

Video Legend (online supplementary content)

Video 1. Wall shear stress (WSS) maps throughout the cardiac cycle for example patients from the 5 study groups. The WSS maps look at the thoracic aorta from 2 different views. Red colour represents areas of high WSS. AR-TAV = aortic regurgitation tricuspid aortic valve; AS-TAV = aortic stenosis tricuspid aortic valve; AS-BAV(RL) = aortic stenosis bicuspid aortic valve with right left cusp fusion; AS-BAV(RN) = aortic stenosis bicuspid aortic valve right non cusp fusion.

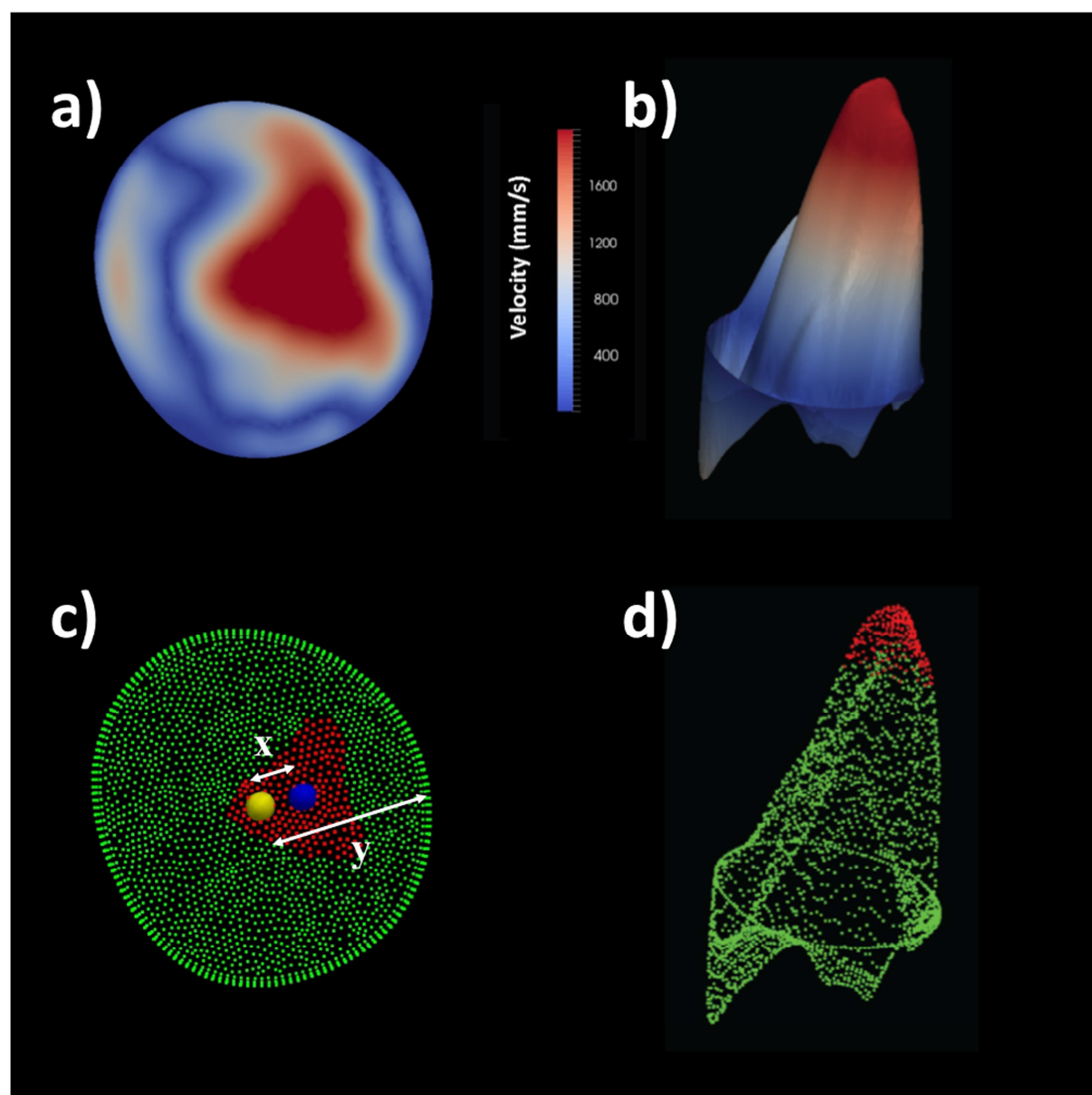
TABLE 1. Demographics, aortic dimensions and hemodynamic indices in the 5 study groups

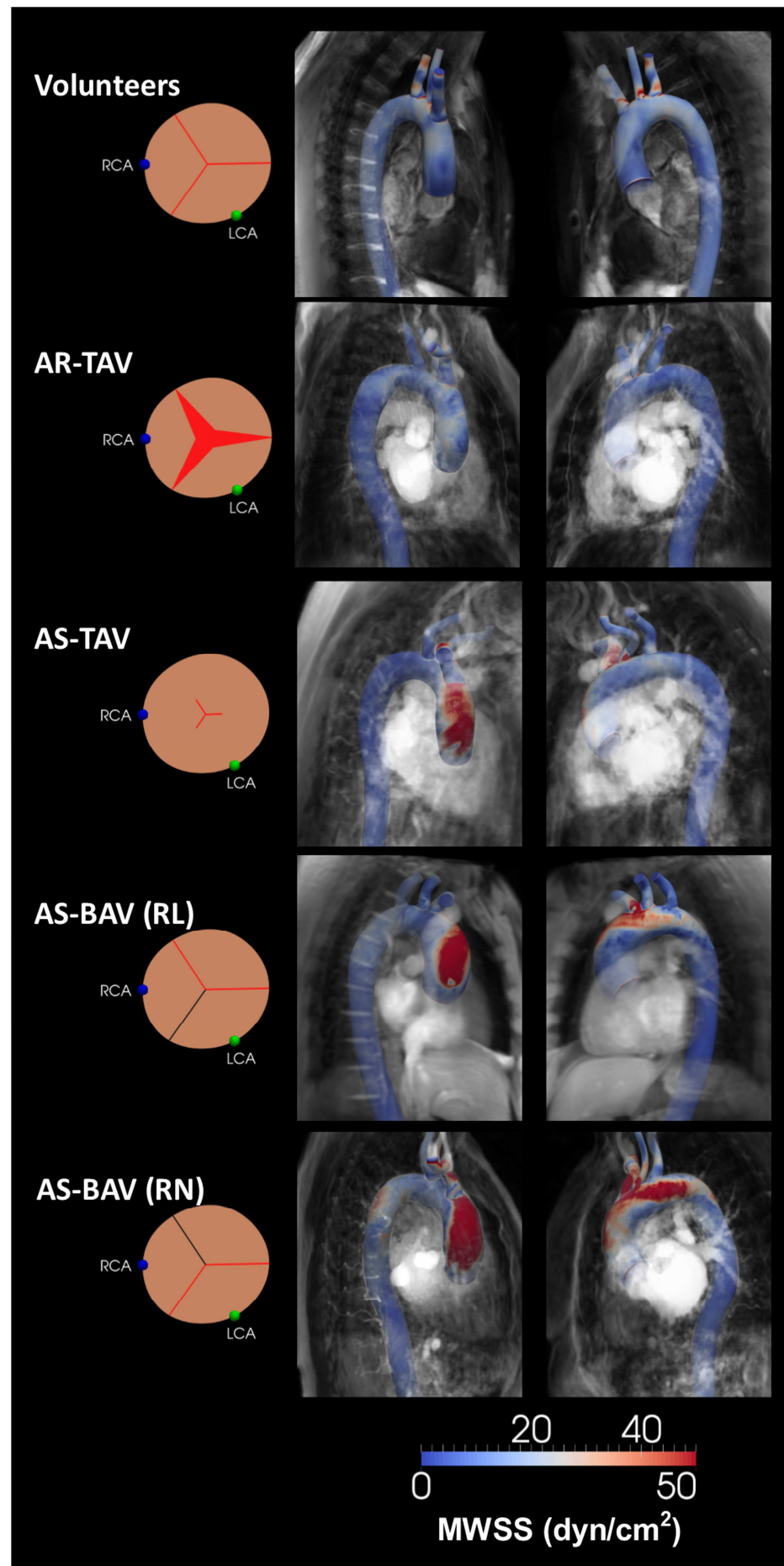
	Volunteers	AR-TAV	AS-TAV	AS-BAV(RL)	AS-BAV(RN)
Demographics					
n	5	10	10	10	10
Male, n (%)	5 (100)	4 (40)	2 (20)	3 (30)	8 (80)
Age	31.3±3.1	54.0±10.8	78.0±1.4*	63.5±7.5*	64.0±8.6
Hypertension	1 (20)	3 (30)	5 (50)	4 (40)	4 (40)
B-Blockers	1 (20)	2 (20)	4 (40)	3 (30)	3 (30)
ACEi / ARBs	1 (20)	2 (20)	5 (50)	3 (30)	4 (40)
Aortic Dimensions (mm)					
SOV diameter	28.8±1.3	33.9±1.9	34.4±2.8	32.2±2.4	35.6±5.1
STJ diameter	22.8±0.9	29.7±1.6	26.3±2.2	29.9±2.7	31.8±2.0
MAA diameter	23.5±1.0	32.4±2.4	32.0±4.3	37.2±4.4*	39.9±2.4*
Hemodynamic Indices					
Flow ^{asymmetry} (%)	4.7±2.1	23.2±5.3	41.1±9.8	72.6±17.2	78.9±6.5†
HFI ^{systole}	0.24±0.02	0.28±0.06	0.26±0.04	0.39±0.04*	0.28±0.03
MWSS ^{Asc Aorta} (dyn/cm ²)	9.8±5.4	17.4±8.8	35.0±20.1	27.3±10.0	37.1±4.0*
OSI ^{Asc Aorta}	0.18±0.04	0.21±0.04	0.19±0.02	0.18±0.03	0.13±0.02

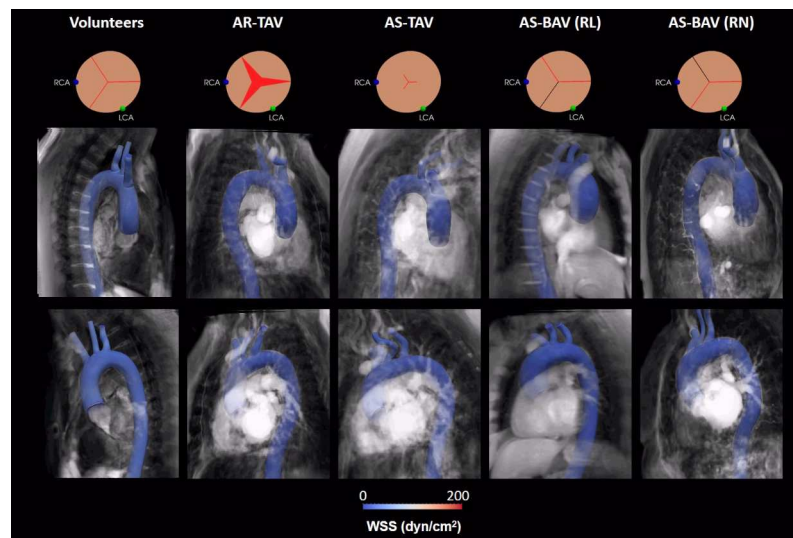
All continuous data are given as mean ± standard deviation. AR-TAV = aortic regurgitation tricuspid aortic valve; AS-TAV = aortic stenosis tricuspid aortic valve; AS-BAV(RL) = aortic stenosis bicuspid aortic valve with right left cusp fusion; AS-BAV(RN) = aortic stenosis bicuspid aortic valve right non cusp fusion; STJ = sinotubular junction; SOV =

584 sinuses of Valsalva; MAA = mid-ascending aorta; HFI = helical flow index; MWSS = mean
585 wall shear stress; OSI = oscillatory shear index; ACEi = angiotensin converting enzyme
586 inhibitor; ARBs = angiotensin II receptor blockers. * denotes significant difference after
587 ANOVA and independent-sample t-test ($p < 0.01$) between the marked group and Volunteers.
588 † denotes significant difference between the marked group and Volunteers, AS-TAV and
589 AR-TAV.

590







Appendix A

MRI Imaging Parameters

Patients underwent standard of care Cardiac Magnetic Resonance (CMR) imaging and Magnetic Resonance Angiography (MRA) to image the entire thoracic aorta, including the head and neck vessels. Gadolinium (0.3 ml/kg; gadodiamide, Omniscan®, GE Healthcare, Waukesha, WI) was infused with a breath-held 3D fast gradient echo sequence using a Philips Achieva 3T scanner (Philips Medical Systems, Eindhoven, Netherlands). Acquired slice thickness was 1.0-2.0 mm, with 56–80 sagittal slices per volume. A 344×344 acquisition matrix was used with a field of view (FoV) of $35 \text{ cm} \times 35 \text{ cm}$ (reconstructed to slices with a spatial resolution of $0.49 \text{ mm} \times 0.49 \text{ mm}$, and resampled to a slice thickness of 1.00 mm). Other parameters included a repetition time (TR) of 3.9 ms, echo time (TE) of 1.4 ms, and a flip angle of 27° .

Time-resolved, velocity encoded 2D anatomic and through-plane PC-MRI (flow MRI) was performed on a plane orthogonal to the ascending aorta at the sino-tubular junction. Heart rates amongst subjects ranged between 50-95 bpm during which 30 images were reconstructed. Imaging parameters included TR, TE, and flip angle of 4.1-4.2 ms, 2.4-2.5 ms, and 15° , respectively. The FoV was $30\text{-}35 \text{ cm} \times 30\text{-}35 \text{ cm}$ with an acquisition matrix of $152\text{-}170 \times 120\text{-}150$, and a slice thickness of 10 mm, resulting in a voxel size of $2.3 \text{ mm} \times 2.4 \text{ mm} \times 10 \text{ mm}$ (resampled at $1.37 \text{ mm} \times 1.36 \text{ mm} \times 10 \text{ mm}$). Data acquisition was carried out within a single breath-hold and gated to the cardiac cycle. Cine sequences were performed for assessment of valve morphology. Velocity sensitivity was set between 150 to 500 cm/s depending on the degree of AS. Average scan times were 20 minutes.

APPENDIX B

Outflow Boundary Conditions

Patient-specific outflow boundary conditions were prescribed at each outlet in the innominate artery, left common carotid artery, left subclavian artery and descending aorta. Upper limb blood pressure was measured after each study using an automated sphygmomanometer cuff with participants in the supine position. A 3 element Windkessel RCR model^{1, 2} was superimposed on each outlet. The Windkessel model represents the arterial tree beyond the model outlet in an intuitive and physiological manner comprising of a proximal resistance (R_p), compliance (C), and a distal resistance (R_d) for each outlet.

R_T is the total resistance in the vascular system. These values were calculated in the following patient-specific manner:

$$R_{total} = \frac{P}{Q}$$

where P = patient's mean arterial pressure, Q = flow, as derived from the PC-MRI inlet velocity profile.

$$R_{total} = \left(\sum_i \frac{1}{R_i} \right)^{-1}$$

and R_i is the total resistance for each individual outlet.

$$R_i = R_p + R_d$$

for each individual outlet, where R_p is proximal resistance, and R_d is the distal resistance. R_i is calculated using the following relationship:

$$\frac{R_{total}}{R_i} = \frac{A_i}{A_T}$$

where A_i is the cross-sectional area of the individual outlet, and A_T is the total cross-sectional area of all outlets in the model. We assumed the ratio of proximal to total resistance:

$$\frac{R_p}{(R_p + R_d)} = 0.056$$

3

Similarly, C_T is the total compliance in the vascular system.

$$C_T = \sum_i C_i$$

and

$$\frac{C_i}{C_T} = \frac{A_i}{A_T}$$

Therefore the flow and compliance at each outlet is proportional to the outlet's area.

Windkessel Parameters

Table 2. Values of the lumped parameter Windkessel boundary conditions for an example patient from each of the 5 groups.

Group	Outlet	Windkessel Parameters		
		R_p	R_d	C
Volunteers	Brachiocephalic Artery	1.36	9.23	48.3
	Left Common Carotid Artery	2.46	15.3	29.2
	Left Subclavian Artery	1.74	11.3	39.3
	Descending Aorta	0.25	2.14	208
AR-TAV	Brachiocephalic Artery	0.41	9.79	22.68
	Left Common Carotid Artery	2.08	39.57	5.61
	Left Subclavian Artery	1.18	24.31	9.13
	Descending Aorta	0.10	2.79	79.58
AS-TAV	Brachiocephalic Artery	0.48	4.91	36.22
	Left Common Carotid Artery	1.73	14.81	12.00
	Left Subclavian Artery	1.65	14.19	12.52
	Descending Aorta	0.19	2.23	79.85
AS-BAV(RL)	Brachiocephalic Artery	0.79	18.2	28.2
	Left Common Carotid Artery	1.15	24.9	20.5
	Left Subclavian Artery	1.29	27.6	18.6
	Descending Aorta	0.17	4.69	109
AS-BAV(RN)	Brachiocephalic Artery	0.67	5.61	49.28
	Left Common Carotid Artery	2.38	16.49	16.77
	Left Subclavian Artery	2.00	14.22	19.45
	Descending Aorta	0.20	2.01	137.90

R_p = proximal resistance; R_d = distal resistance; C = capacitance. The units of resistance are 10^3 dynes s / cm⁵. The units of capacitance are 10^{-6} cm⁵ / dynes.

References

1. Figueroa CA, Vignon-Clementel IE, Jansen KC, Hughes TJ and Taylor CA. A coupled momentum method for modeling blood flow in three-dimensional deformable arteries. *Comput Methods Appl Mech Eng.* 2006;195:5685-5706.
2. Vignon-Clementel IE FC, Jansen KE, Taylor CA. Outflow boundary conditions for three-dimensional finite element modeling of blood flow and pressure in arteries. *Comput Methods Appl Mech Eng.* 2006;195:3776-3796.
3. Laskey WK, Parker HG, Ferrari VA, Kussmaul WG and Noordergraaf A. Estimation of total systemic arterial compliance in humans. *J Appl Physiol.* 1990;69:112-9.

APPENDIX C

Haemodynamic Indices

Helical Flow Index

Aortic 3D velocity streamlines were calculated from temporally resolved velocity data for the entire thoracic aorta, and colour coded to represent blood velocity. Helicity is a metric that represents the extent to which corkscrew-like motion occurs, and is governed by velocity and vorticity.¹ Helical Flow Index (HFI) was calculated to quantitatively measure the degree of helicity. HFI_p is the helical flow index for each pathline (velocity streamline), calculated over the particle trajectory:

$$HFI_p = \frac{1}{N_j} \sum_i^{N_j} \psi_i$$

Here, ψ_i is the dimensionless normalised helicity, calculated as the cosine of the angle between velocity and vorticity vectors at each point of the pathline. N_j is the number of 0.5mm steps, $i = 1, \dots, N_j$, along the fluid particle pathline j . Steady Poiseuille flow gives a value of $\psi_i = 0$, whereas values of $|\psi| = 1$ occur when flow is purely helical.^{1, 2} $HFI_{systole}$ is the average HFI_p over all pathlines during peak systole.

Wall Shear Stress

WSS expresses the force per unit area exerted by a flowing fluid on a surface of the lumen in the direction of the local tangent. In a complex 3D geometry such as the aorta, wall shear stress \overrightarrow{WSS} can be obtained as follows:

$$\overline{WSS} = \mu(\nabla \vec{u} + \nabla \vec{u}^T) \vec{n}$$

where μ is the blood viscosity, $\nabla \vec{u}$ is the gradient of the velocity field, $\nabla \vec{u}^T$ is the transpose of the gradient of the velocity field, and \vec{n} is the unit normal vector to the vessel wall.

Oscillatory Shear Index

In pulsatile flow, the temporal variation in WSS direction can be expressed in terms of the OSI:

$$OSI = \frac{1}{2} \left(1 - \frac{|\int_0^T WSS_z dt|}{\int_0^T |WSS_z| dt} \right)$$

1

where an OSI value of zero indicates unidirectional flow throughout the pulsatile cycle, and a value of 0.5 indicates that flow oscillates forward and backward for the same period of time during the cycle (i.e. disturbed flow). OSI essentially measures the degree of disturbed flow at the vessel wall,¹ and has been shown to be associated with vasculopathy.¹

References

1. Hardman D, Semple SI, Richards JM and Hoskins PR. Comparison of patient-specific inlet boundary conditions in the numerical modelling of blood flow in abdominal aortic aneurysm disease. *Int J Numer Method Biomed Eng.* 2013;29:165-78.
2. Morbiducci U, Ponzini R, Rizzo G, Cadioli M, Esposito A, De Cobelli F, et al. In vivo quantification of helical blood flow in human aorta by time-resolved three-dimensional cine phase contrast magnetic resonance imaging. *Ann Biomed Eng.* 2009;37:516-31.